Analysis on the attitude dynamics of a PhoneSat during deployment

Qiao Qiao, Jianping Yuan and Xin Ning
School of Astronautics, Northwestern Polytechnical University, Xi'an,
China and National Key Laboratory of Aerospace Flight Dynamics, Xi'an, China

Abstract

Purpose – The purpose of this paper is to establish the dynamics model of a Z-folded PhoneSat considering hinge friction and to investigate the influence of disturbances, such as friction, stiffness asymmetry, deployment asynchronicity and initial disturbance angular velocity, on the attitude of PhoneSat during and after deployment.

Design/methodology/approach – For the Z-folded PhoneSat, the dynamics model considering hinge friction is established and the dynamics simulation is carried out. The effects of friction, stiffness asymmetry, deployment asynchronicity and initial disturbance angular velocity on the attitude motion of the PhoneSat are studied and the attitude motion regularities of the PhoneSat considering the disturbance factors mentioned above are discussed.

Findings – Friction has a main contribution to reducing the oscillation of attitude motion and damping out the residual oscillation, ultimately decreasing the deployment time. An increasing length of deployment time is required with the increasing stiffness asymmetry and time difference of asynchronous deployment, which also have slight disturbances on the attitude angle and angular velocity of PhoneSat after the deployment. The initial disturbance angular velocity in the direction of deployment would be proportionally weakened after the deployment, whereas initial disturbance angular velocity in other direction induces angular velocities of other axes, which dramatically enhances the complexity of attitude control.

Originality/value – The paper is a useful reference for engineering design of small satellites attitude control system.

Keywords Attitude motion, PhoneSat, Spring-deployed deployment

Paper type Case study

Introduction

In recent years, nanosatellites have attracted great attention because of their low cost, short development lifecycle and promising applications (Cockrell *et al.*, 2012; Heidt *et al.*, 2000; Piattoni *et al.*, 2012). Sufficient power supply is the most essential factor for the operation of small satellites, but it is restricted by the limited surface area for mounting solar cells. Hence, deployable solar panels have been adopted as an efficient on-board power generation solution without substantially increasing the volume of the satellite (Plaza *et al.*, 2010), whereas other ways to increase available power do not prove to be extremely excellent in performance (Jansen *et al.*, 2010; Santoni and Piergentili, 2008).

The deployable solar panels of large spacecraft have been studied extensively (Fufa *et al.*, 2010; Gao *et al.*, 2008; Kote *et al.*, 2007; Wallrapp and Wiedemann, 2002; Wie *et al.*, 1986) in the past years. However, the well-studied solar panel deployment of large satellite cannot be directly applied to miniaturized satellites because of their typically strict volume, mass and mechanisms size constrains. Specifically, motor driving systems and hinge locking mechanisms, prevalent in solar panel deployment of large spacecraft (Calassa and Kackley, 1995; Campbell *et al.*, 2006; Gerlach *et al.*, 1990; Lee, 2005), are not suitable for nanosatellites. Rather, passively deployed solar arrays, utilizing preloaded torsion springs as the actuators of rotation movement, have grown in popularity owing to their unique characteristic of light weight, compact volume and simple design (Clark and Kirk, 2012; Jaeger *et al.*, 2011; Plaza *et al.*, 2010; Reif *et al.*, 2010; Santoni *et al.*, 2014).

However, the literature (Clark and Kirk, 2012; Jaeger *et al.*, 2011; Plaza *et al.*, 2010; Reif *et al.*, 2010; Santoni *et al.*, 2014) mentioned above studied the deployment of solar panels in the conventional mode, that is, the solar panels are deployed ideally, without considering disturbances, such as stiffness asymmetry, deployment asynchronicity, friction and initial disturbance angular velocity. In fact, asymmetric stiffness parameters of torsion springs are inevitable because of manufacturing errors, which may influence the attitude motion of spacecraft after deployment (Santoni, 2014). Moreover, small satellites with deployable appendages are highly vulnerable to asynchronous deployment owing to the absence of synchro-mechanism to ensure a sufficient level of deployment synchronicity. Hence, unsynchronized deployment of solar panel arrays because of the slight variation of the

The current issue and full text archive of this journal is available on Emerald Insight at: **www.emeraldinsight.com/1748-8842.htm**

Aircraft Engineering and Aerospace Technology: An International Journal
89/3 (2017) 498–506

[DOI 10.1108/AEAT-01-2016-0013]

The authors are grateful for the support and funding from National Science Foundation of China (No. 11402200, X. Ning).

Received 18 January 2016
Revised 30 March 2016
Accepted 31 March 2016

Aircraft Engineering and Aerospace Technology: An International Journal
Volume 89 · Number 3 · 2017 · 498–506

release time of the torsion springs would significantly modify the projected attitude motion. In addition, friction in joints and initial disturbance angular velocity induced by the releasing process from the launch vehicle may also interfere with the deployment process of the small spacecraft, which eventually lead to significant deviations between the anticipative deployment and the real outcome.

To eliminate the perturbation, the most common approach is to correct the attitude disturbance after deployment, which consumes more energy during the reorientation and imposes strict requirements on pointing accuracy. By contrast, we introduce a novel concept called virtual attitude correction which is especially suitable for nanosatellites with limited control ability and power but possessing powerful capability of calculation. Specifically, the influence of disturbance factors would be theoretically analyzed, and the actual post-deployment attitude under the influence of those disturbance factors would be computed by the virtual attitude correction system based on the analytical model established in this paper and regarded as the current attitude instead of correcting it, potentially avoiding the complex procedure of adjusting the attitude deviation after the deployment. For the future maneuver, the updated current attitude of the nanosatellite would be calculated by the virtual attitude correction system according to the maneuver it takes, which indicates that the whole process of attitude determination is carried out purely from a virtual platform rather than an actual attitude determination system, eliminating the need of the assembly of attitude determination system and the correction of the attitude deviation. This strategy guarantees that nanosatellites could function properly even without the attitude correction. For example, nanosatellites equipped with cameras could mark each photograph it takes with current attitude information obtained from the virtual attitude correction system.

The research developed in this paper refers in particular to a foldable picosatellite called NPU-PhoneSat proposed by Yuan *et al.* (2015). The objective of this paper is to study the effect of friction, stiffness asymmetry, asynchronous deployment and initial disturbance angular velocity on the deployment, with the purpose of providing valuable data of the post-deployment attitude. This paper is organized as follows: the second section presents the dynamic model of NPU-PhoneSat. In the third section, simulations of deployment of PhoneSat are presented, analyzing the influence of friction, stiffness asymmetry, asynchronous deployment and initial disturbance angular velocity on the attitude motion and the post-deployment attitude. Finally, the fourth section ends the paper with the concluding remarks.

Dynamics of NPU-PhoneSat

The NPU-PhoneSat is analyzed in this paper, which is specially designed as a foldable platform with multiple-slice for a better incorporation of COTS smart phone components. As shown in Figure 1, it allows a compact structure during launching and supports a self-unfolding behavior in space. The modular deployable NPU-PhoneSat consists of three identical rectangular rigid bodies connected by rotary hinges in a chain, with the ability of scaling up or reconfiguring with different functional modules. For convenience of the following

Figure 1 PhoneSat in the folded and deployed state

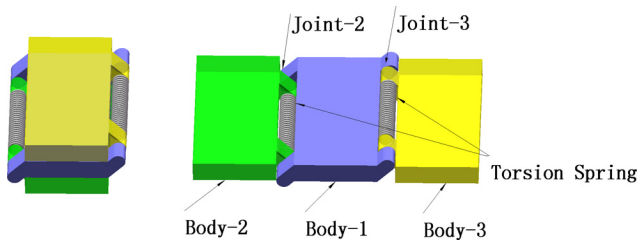

analysis, three rigid bodies connected in a chain from left to right when deployed are named "Body-2", "Body-1" and "Body-3", respectively, as illustrated in Figure 1. The joint connecting the Body-1 and the Body-2 is defined as Joint-2, whereas the other one connecting the Body-1 and the Body-3 is defined as Joint-3. Torsion springs located in Joint-2 and Joint-3 act as the actuators of the rotation movement at each rotary hinge.

The dynamic model of the spring deployed NPU-PhoneSat is established based on the recursive method, characterized by the utilization of relative coordinates of hinges to describe the configuration of the system (Hong, 1999). As shown in Figure 2, four sets of coordinates are defined. The coordinates $X_0Y_0Z_0$ is inertial frame. The other three coordinates are the body-fixed ones, namely, the Body-1 coordinates $X_1Y_1Z_1$, the Body-2 coordinates $X_2Y_2Z_2$ and the Body-3 coordinates $X_3Y_3Z_3$, whose origins are, respectively, fixed to the mass centers of bodies and the X-, Y- and Z-axis are along the length-, width- and thick-edge of bodies, respectively.

As the attitude of system during the deployment is the focus of this paper, a fictitious spherical joint named Joint-1 is assumed between the Body-1 and the inertial frame, ignoring the position change of the PhoneSat. Therefore, the overall configuration of the NPU-PhoneSat composed of three bodies could be completely defined by three Euler angles of the Body-1 with respect to the inertial frame, $\boldsymbol{q}_1 = [\theta_1, \theta_2, \theta_3]^T$, which respectively, rotate through X_0-, Y_0- and Z_0-axis and two relative rotation angles in Joint-2 and Joint-3, namely, $\boldsymbol{q}_2$ and $\boldsymbol{q}_3$. Hence, the set of generalized coordinates $\boldsymbol{q} = [\boldsymbol{q}^T_1, \boldsymbol{q}^T_2, \boldsymbol{q}^T_3]^T$ is selected to describe the rotational motion of the system. The equations

Figure 2 Model of the PhoneSat and four coordinates

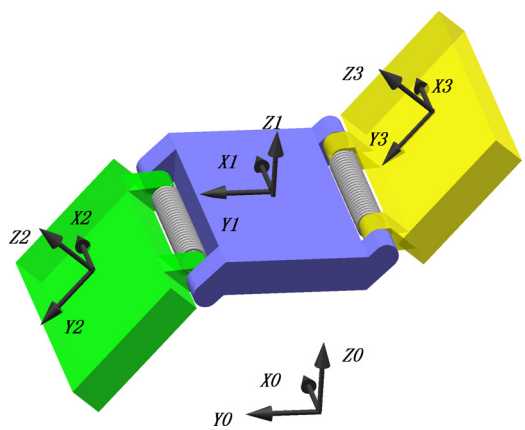

of motion can be readily derived by the standard procedure of modelling (Hong, 1999).

Relative motion of the joints

Define:

$$\boldsymbol{H}_1^{\Omega T} = [\boldsymbol{p}_{11}, \boldsymbol{p}_{12}, \boldsymbol{p}_{13}]$$

$$\boldsymbol{\eta}_1 = \boldsymbol{p}_{11} \times \boldsymbol{p}_{12}\dot{\theta}_{M1}\dot{\theta}_{M2} + \boldsymbol{p}_{11} \times \boldsymbol{p}_{13}\dot{\theta}_{M1}\dot{\theta}_{M3} + \boldsymbol{p}_{12} \times \boldsymbol{p}_{13}\dot{\theta}_{M2}\dot{\theta}_{M3}$$

The relative angular velocity vector and relative angular acceleration vector of Joint-1 can be written as:

$$\boldsymbol{\omega}_{r1} = \boldsymbol{H}_1^{\Omega T}\dot{\boldsymbol{q}}_1 \tag{1}$$

$$\frac{{}^{r}d}{dt}\boldsymbol{\omega}_{r1} = \boldsymbol{H}_1^{\Omega T}\ddot{\boldsymbol{q}}_1 + \boldsymbol{\eta}_1 \tag{2}$$

Similarly, the relative angular velocity vector and relative angular acceleration vector of Joint-2 and Joint-3 can be described as:

$$\boldsymbol{\omega}_{r2} = \boldsymbol{p}_2\dot{q}_2 = \boldsymbol{H}_2^{\Omega T}\dot{q}_2 \tag{3}$$

$$\frac{{}^{r}d}{dt}\boldsymbol{\omega}_{r2} = \boldsymbol{p}_2\ddot{q}_2 = \boldsymbol{H}_2^{\Omega T}\ddot{q}_2 + \boldsymbol{\eta}_2 \tag{4}$$

where $\boldsymbol{\eta}_2 = 0$ and $\boldsymbol{H}_2^{\Omega T} = \boldsymbol{p}_2$ is the unit vector of the rotation axis of Joint-2:

$$\boldsymbol{\omega}_{r3} = \boldsymbol{p}_3\dot{q}_3 = \boldsymbol{H}_3^{\Omega T}\dot{q}_3 \tag{5}$$

$$\frac{{}^{r}d}{dt}\boldsymbol{\omega}_{r3} = \boldsymbol{p}_3\ddot{q}_3 = \boldsymbol{H}_3^{\Omega T}\ddot{q}_3 + \boldsymbol{\eta}_3 \tag{6}$$

where $\boldsymbol{\eta}_3 = 0$ and $\boldsymbol{H}_3^{\Omega T} = \boldsymbol{p}_3$ is the unit vector of the rotation axis of Joint-3.

Relative motion of the system

The relative angular velocity vector of the system is given by:

$$\boldsymbol{\omega}_r = \boldsymbol{H}^{\Omega T}\dot{q} \tag{7}$$

where $\boldsymbol{\omega}_r = [\boldsymbol{\omega}_{r1}, \boldsymbol{\omega}_{r2}, \boldsymbol{\omega}_{r3}]^T$, $H^{\Omega T} = diag(\boldsymbol{H}_1^{\Omega T}, \boldsymbol{H}_2^{\Omega T}, \boldsymbol{H}_3^{\Omega T})$.

Similarly, the relative angular acceleration vector of the system is given by:

$$\frac{{}^{r}d}{dt}\boldsymbol{\omega}_r = \boldsymbol{H}^{\Omega T}\ddot{\boldsymbol{q}} + \boldsymbol{\eta} \tag{8}$$

where ${}^{r}d/dt\boldsymbol{\omega}_r = [{}^{r}d/dt\boldsymbol{\omega}_{r1}, {}^{r}d/dt\boldsymbol{\omega}_{r2}, {}^{r}d/dt\boldsymbol{\omega}_{r3}]^T$, $\boldsymbol{\eta} = [\boldsymbol{\eta}_1, \boldsymbol{\eta}_2, \boldsymbol{\eta}_3]^T$.

Absolute motion of the system

The relationship between the absolute angular velocity vector of the system, $\boldsymbol{\omega} = [\boldsymbol{\omega}_1, \boldsymbol{\omega}_2, \boldsymbol{\omega}_3]^T$, and the relative angular velocity vector of the system, $\boldsymbol{\omega}_r = [\boldsymbol{\omega}_{r1}, \boldsymbol{\omega}_{r2}, \boldsymbol{\omega}_{r3}]^T$, can be written as:

$$\boldsymbol{\omega} = -T^T\boldsymbol{\omega}_r \tag{9}$$

where T is the channel matrix of the system, which is defined as:

$$T = \begin{pmatrix} -1 & -1 & -1 \\ 0 & -1 & 0 \\ 0 & 0 & -1 \end{pmatrix}$$

By substituting equation (7) into equation (9), we can obtain the relationship between the absolute angular velocity vector of the system and the system's generalized coordinates, which is given by:

$$\boldsymbol{\omega} = \boldsymbol{\beta}\dot{q} \tag{10}$$

where $\boldsymbol{\beta} = -(\boldsymbol{H}^{\Omega}T)^T$. Thus, the angular velocity variation can be written as:

$$\Delta\boldsymbol{\omega} = \boldsymbol{\beta}\Delta\dot{\boldsymbol{q}} \tag{11}$$

The relationship between the absolute angular acceleration vector of the system and the system's generalized coordinates can be given by:

$$\dot{\boldsymbol{\omega}} = \boldsymbol{\beta}\ddot{\boldsymbol{q}} + \boldsymbol{\sigma} \tag{12}$$

where $\boldsymbol{\sigma} = -T^T(\boldsymbol{\eta}+\boldsymbol{\zeta})$, $\xi = [\xi_1, \xi_2, \xi_3]^T = [0, \boldsymbol{\omega}_1 \times \boldsymbol{\omega}_{r2}, \boldsymbol{\omega}_1 \times \boldsymbol{\omega}_{r3}]^T$.

The relationship between the center-of-mass velocities of three bodies and the generalized coordinates can be given by:

$$\dot{\boldsymbol{r}} = \boldsymbol{\alpha}\dot{\boldsymbol{q}} \tag{13}$$

where $\dot{\boldsymbol{r}} = [\dot{\boldsymbol{r}}_1, \dot{\boldsymbol{r}}_2, \dot{\boldsymbol{r}}_3]^T\boldsymbol{\alpha} = -(\boldsymbol{H}^{\Omega}T \times \boldsymbol{d})^T$ *and* $\boldsymbol{d} = \begin{pmatrix} \boldsymbol{0} & \boldsymbol{d_{12}} & \boldsymbol{d_{13}} \\ \boldsymbol{0} & \boldsymbol{d_{22}} & \boldsymbol{0} \\ \boldsymbol{0} & \boldsymbol{0} & \boldsymbol{d_{33}} \end{pmatrix}$. Thus, the variation of the center-of-mass velocities of three bodies can be written as:

$$\Delta\dot{\boldsymbol{r}} = \boldsymbol{\alpha}\Delta\dot{\boldsymbol{q}} \tag{14}$$

Similarly, the center-of-mass accelerations of three bodies can be rewritten in the matrix form:

$$\ddot{\boldsymbol{r}} = -\boldsymbol{d}^T \times \dot{\boldsymbol{\omega}} + \boldsymbol{u}$$

where:

$$\boldsymbol{u}_1 = 0$$

$$\boldsymbol{u}_2 = \boldsymbol{\omega}_1 \times (\boldsymbol{\omega}_1 \times \boldsymbol{d}_{12}) + \boldsymbol{\omega}_2 \times (\boldsymbol{\omega}_2 \times \boldsymbol{d}_{22})$$

$$\boldsymbol{u}_3 = \boldsymbol{\omega}_1 \times (\boldsymbol{\omega}_1 \times \boldsymbol{d}_{13}) + \boldsymbol{\omega}_3 \times (\boldsymbol{\omega}_3 \times \boldsymbol{d}_{33})$$

By substituting equation (12) into equation (15), the relationship between the center-of-mass accelerations of three bodies and the generalized coordinates can be obtained as following:

$$\ddot{\boldsymbol{r}} = \alpha\ddot{\boldsymbol{q}} + \boldsymbol{w} \tag{16}$$

where $\boldsymbol{w} = \boldsymbol{u} - \boldsymbol{d}^T \times \boldsymbol{\sigma}$.

Constraint force element

The constraint force element of the NPU-PhoneSat system includes the spring torque and the hinge friction acting on Joint-2 and Joint-3.

The torque provided by the torsion spring in the Joint-*i* (*i* = 2,3) can be represented by equation (17) as follows:

$$\tau_{spring,i} = k_i(q_{i0} - q_i) - c_i\dot{q}_i \tag{17}$$

where k_i and c_i are the torque constant and damping constant of the torsion spring in Joint-*i*, respectively; q_{i0} is the free angle of the spring; and q_i and $\dot{q}_i$ are the angular displacement and angular velocity of Joint-*i*, respectively.

In addition to the spring torque, the hinge friction damping torque existing in Joint-2 and Joint-3 can be determined according to the dynamic and static hinge friction models.

The torque caused by the static friction in Joint-*i* (*i* = 2, 3) can be defined as:

$$\tau_{f,statici} = r_s\left(\mu_s\frac{\tau_{spring\,i}(t=0)}{r_l}\right)\delta(t) \tag{18}$$

where r_s is the radius of the hinge shaft, μ_s is the static friction coefficient, $\tau_{springi}(t = 0)$ is the total torque provided by the spring in Joint-*i* at the initial moment and r_l is the torsion spring leg length.

The dynamic friction is related to the normal force at the point of contact, which reacts to the centripetal force caused by the rotation motion of the cover. Thus, the torque induced by the dynamic friction can be represented as a function of the square of the angular velocity of the Joint-*i* (*i* = 2, 3), that is:

$$\tau_{f,\,dyn,\,i} = r_s(\mu_d m r_{CM}\dot{q}_i^{\,2}) \tag{19}$$

where μ_d is the dynamic friction coefficient, m is the mass of the panel and r_{CM} is the distance from the axis of rotation to the mass center of the panel.

Hence, the total torque acting on Joint-*i* can be written as:

$$\tau_{total,i} = \tau_{spring,i} + \tau_{fi} + \tau_{fi,\,dyn,\,i} \tag{20}$$

From the above, the generalized force corresponding to the generalized coordinates of the system can be written as:

$$\boldsymbol{F}^c = [\boldsymbol{0}, \tau_{total2}, \tau_{total3}]^T = [0, 0, 0, \tau_{total2}, \tau_{total3}]^T \tag{21}$$

Then, the virtual power can be obtained as:

$$\Delta P = \Delta\dot{\boldsymbol{q}}^T \cdot \boldsymbol{F}^c \tag{22}$$

Dynamic equation of NPU-PhoneSat deployment

The generalized equation of dynamics in the form of virtual power principle can be written as:

$$\sum_{i=1}^{3}[\Delta\dot{\boldsymbol{r}}_i \cdot (-m_i\ddot{\boldsymbol{r}}_i + \boldsymbol{F}_i^o) + \Delta\boldsymbol{\omega}_i \cdot (-\boldsymbol{J}_i \cdot \dot{\boldsymbol{\omega}}_i - \boldsymbol{\varepsilon}_i + \boldsymbol{M}_i^o)] + \Delta P = 0 \tag{23}$$

where $\boldsymbol{\varepsilon}_i = \boldsymbol{\omega}_i \times (\boldsymbol{J}_i \cdot \boldsymbol{\omega}_i)$. m_i and $\boldsymbol{J}_i$ are the mass and inertia tensor of Body-*i* (*i* = 1, 2, 3), respectively. $\boldsymbol{F}_i^o$ and $\boldsymbol{M}_i^o$ are the external force and moment acting on the center of mass of Body-*i*, respectively.

From equation (23), the dynamic equation of the system can be written in the matrix form as:

$$\Delta\dot{\boldsymbol{r}}^T \cdot (-\boldsymbol{m} \cdot \ddot{\boldsymbol{r}} + \boldsymbol{F}^o) + \Delta\boldsymbol{\omega}^T \cdot (-\boldsymbol{J} \cdot \dot{\boldsymbol{\omega}} - \boldsymbol{\varepsilon} + \boldsymbol{M}^o) + \Delta P = 0 \tag{24}$$

where $\boldsymbol{m} = diag(m_1, m_2, m_3)$, $\boldsymbol{J} = diag(\boldsymbol{J}_1, \boldsymbol{J}_2, \boldsymbol{J}_3)$, $\boldsymbol{F}^o = [\boldsymbol{F}_1^o, \boldsymbol{F}_2^o, \boldsymbol{F}_3^o]^T$, $\boldsymbol{M}^o = [\boldsymbol{M}_1^o, \boldsymbol{M}_2^o, \boldsymbol{M}_3^o]^T$ and $\boldsymbol{\varepsilon} = [\boldsymbol{\varepsilon}_1, \boldsymbol{\varepsilon}_2, \boldsymbol{\varepsilon}_3]^T$. Because the PhoneSat is free-floating on orbit, there is no external force and moment acting on the system during the deployment, thus:

$$\boldsymbol{F}^o = \boldsymbol{0} \tag{25}$$

$$\boldsymbol{M}^o = \boldsymbol{0} \tag{26}$$

By substituting equations (10) (11), (12), (14), (16), (22), (25) and (26) into equation (24), it can be rewritten as:

$$\Delta\dot{\boldsymbol{q}}^T(-\boldsymbol{Z}\ddot{\boldsymbol{q}} + \boldsymbol{z}) = 0 \tag{27}$$

where $\boldsymbol{Z} = \boldsymbol{\alpha}^T \cdot \boldsymbol{m} \cdot \boldsymbol{\alpha} + \boldsymbol{\beta}^T \cdot \boldsymbol{J} \cdot \boldsymbol{\beta}$, $\boldsymbol{z} = -\boldsymbol{\alpha}^T \cdot \boldsymbol{m} \cdot \boldsymbol{w} + \boldsymbol{\beta}^T \cdot (-\boldsymbol{J} \cdot \boldsymbol{\sigma} - \boldsymbol{\varepsilon}) + \boldsymbol{F}^c$.

Because the velocity variations of the generalized coordinates are independent from each other, the dynamic equation of the system can be given as:

$$\boldsymbol{Z}\ddot{\boldsymbol{q}} = \boldsymbol{z} \tag{28}$$

where q is the generalized coordinate column matrix which is defined as $\boldsymbol{q} = [\theta_{M1}, \theta_{M2}, \theta_{M3}, q_2, q_3]^T$, $\boldsymbol{Z}$ is a 5 × 5 generalized mass matrix and z is a 5 × 1 generalized force column matrix.

Numerical simulation of NPU-PhoneSat deployment

Properties of the NPU-PhoneSat

Figure 2 shows the configuration of the NPU-PhoneSat, which consists of three rigid bodies connected by revolute joints, being almost the same size as the cell phone when folded. The deployment of the PhoneSat is driven by the torsion spring in joint.

At the beginning, the NPU-PhoneSat is in the folding state. For the sake of simplicity, three rigid bodies of the PhoneSat are considered to be identical and mass, geometric and inertia parameters of each body are shown in Table I. Table II

Table I Geometric and mass properties of the PhoneSat

Parameters	Value
Mass (kg)	0.1
Length (m)	0.16
Width (m)	0.08
Height (m)	0.02
Jx (kg m^2)	5.7×10^{-5}
Jy (kg m^2)	2.2×10^{-4}
Jz (kg m^2)	2.7×10^{-4}
Jxy (kg m^2)	0
Jyz (kg m^2)	0
Jzx (kg m^2)	0

Table II Parameters of the revolute joint

Parameters	Value
Free angle of torsion spring (q_0) (deg.)	180
Stiffness coefficient of torsion spring (k) (Nm/deg.)	1×10^{-4}
Damping coefficient of torsion spring (c) (N ms/deg.)	1×10^{-6}
Radius of the hinge shaft (r_s) (m)	4×10^{-3}
Torsion spring leg length (r_l) (m)	1×10^{-2}
Static friction coefficient (μ_d)	0.2
Dynamic friction coefficient (μ_d)	0.3

presents the parameters of the revolute joint used in the simulation of deployment.

In the following, four different simulations are presented and analyzed. At the beginning, simulations were carried out with and without friction, with the assumption that parameters of Joint-2 and Joint-3 are perfectly consistent utilizing the parameters shown in Table II. The other three simulations are implemented to explore the effect of asymmetric stiffness, asynchronous deployment and the initial disturbance angular velocity.

Effect of friction on the deployment of PhoneSat

Figure 3 presents the attitude angles and angular velocities of three panels of the PhoneSat during the deployment with and without friction. As can be seen from Figure 3, friction seems to have a noticeable impact on the deployment dynamics of the PhoneSat. At the beginning of the deployment, in the case of considering friction, attitude angle of all the three panels are oscillating steadily as the panels deploy, with the oscillating amplitude gradually decreasing, owing to the damping of the torsion spring and the friction. Until the time t = 6.25 s, the three panels deploy completely, and the attitude of the PhoneSat tends to be stable. The most obvious difference between the two cases, i.e. with and without friction, is that the oscillating amplitude without friction is obviously larger than that with friction because friction consumes mechanical energy. Moreover, it can also be found that friction has slight effect on the deployment time. The PhoneSat deploys completely at time t = 6.25 s when considering friction, whereas the deployment time without friction is t = 8.5 s, extending the deployment time for 2.25 s. From the angular velocity of the PhoneSat shown in Figures 3 (b), (d) and (f), it can be observed that the angular velocity without friction varies more intensely with higher peaks of angular velocity, compared with the case considering friction.

The other point to be noticed is that the attitude after the deployment considering friction is almost the same as the post-deployment attitude without friction. Thus, it can be concluded that the existence of friction has a significant influence on the process of the deployment while has little effect on the post-deployment attitude.

Effect of asymmetric torsion spring stiffness coefficient on the deployment of PhoneSat

The assumption of perfectly consistent values of spring coefficient leads to the ideal deployment, with the deployment response of the external panels, i.e. Body-2 and Body-3, being the same. However, slight variations of torsion spring stiffness coefficients are inevitable owing to the manufacturing error, which would cause the unexpected interactions between the panels. To investigate the effects of asymmetric stiffness coefficient of torsion spring on the deployment of the PhoneSat, this section presents the simulation results of four cases in which the stiffness of torsion spring in Joint-2 is increased at steps of 10 per cent starting from 0 to 30 per cent, whereas the stiffness of spring in Joint-3 remains unaltered. The simulation results are shown in Figure 4.

Figure 4 (a), (c) and (e) shows the attitude angles of Body-1, Body-2 and Body-3 during the deployment with symmetric and asymmetric stiffness coefficient of spring, respectively. As shown in the figure, inconsistent value of stiffness has extraordinarily obvious influence on the deployment time. With symmetric stiffness, the PhoneSat requires 6.25 s to be deployed completely, whereas with inconsistent stiffness, the PhoneSat requires 17 and 19.25 s to complete the deployment when the stiffness difference is 10 and 20 per cent, respectively. When it comes to the stiffness difference of 30 per cent, it takes more than 20 s to achieve the fully deployment because of the residual oscillation caused by the coupling of three panels. It

Figure 3 Attitude motion of the PhoneSat

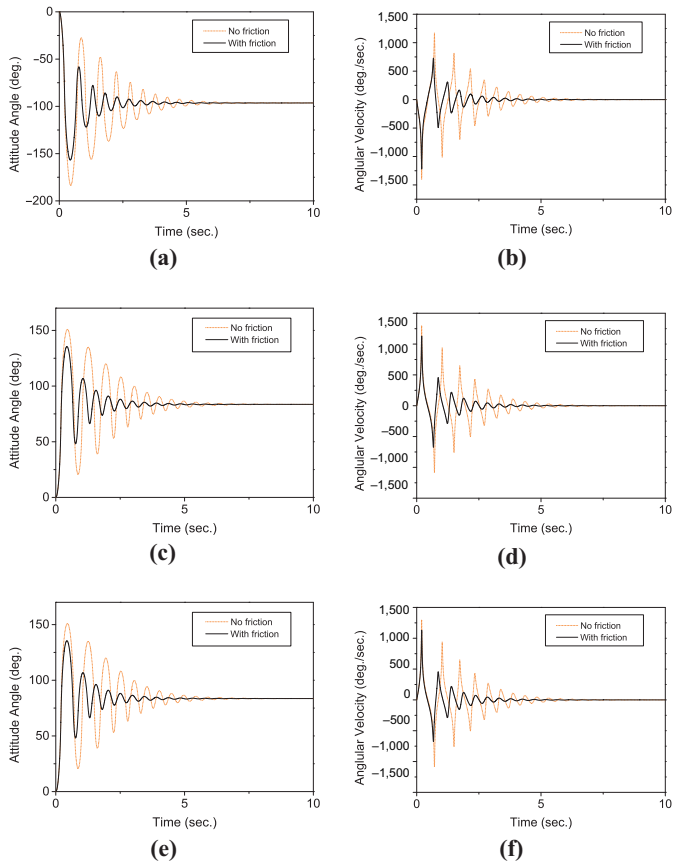

Notes: (a), (c) and (e) are the attitude angles of Body-1, Body-2 and Body-3, respectively; (b), (d) and (f) are the angular velocities of Body-1, Body-2 and Body-3, respectively

Figure 4 Attitude angles of the PhoneSat

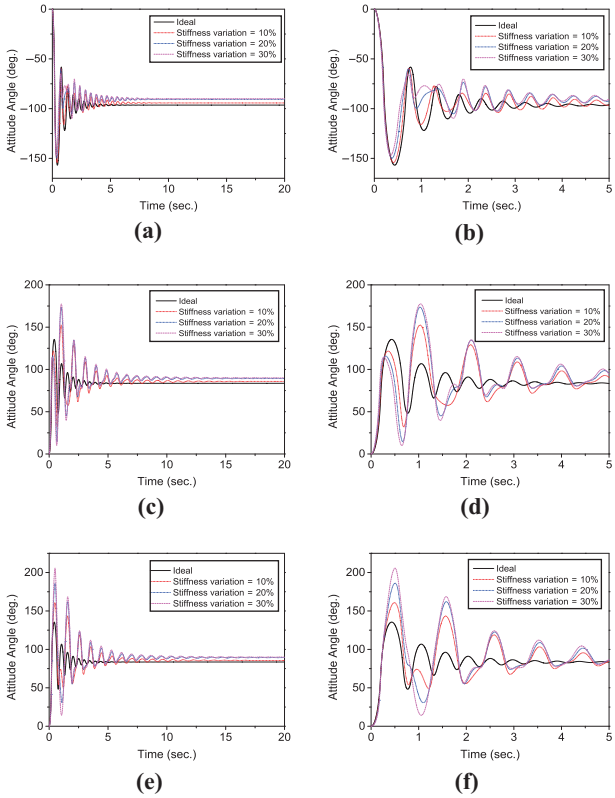

Notes: (a), (c) and (e) are the whole process drawings of Body-1, Body-2 and Body-3, respectively; (b), (d) and (f) are the partial enlarged drawings of the beginning of the deployment of Body-1, Body-2 and Body-3, respectively

indicates that the PhoneSat requires an increasing length of time for the complete deployment with increasing difference of the stiffness of torsion springs.

Moreover, it can be seen that the variation of stiffness has slight effect on the attitude of the PhoneSat after the deployment is completed, and the final attitude is deflected from the ideal condition, with the maximum difference in the order of 10°. It can also be observed that the larger the stiffness difference between the revolute joints of PhoneSat, the larger variation of the attitude angle at the end of the deployment process with respect to the case of consistent stiffness.

As can be seen in the partial enlarged drawing of the first 5 s, i.e. Figure 4 (b), (d) and (f), higher levels of oscillation of attitude exist for conditions involving a larger difference in spring stiffness of the two joints. However, compared with the two external panels, i.e. Body-2 and Body-3, the internal panel seems to be less sensitive to the inconsistence of the stiffness. These higher levels of oscillation affect the steadiness of the deployment process and degrade the performance of the sensitive devices. With an even larger stiffness difference of the revolute joints, the oscillation of the deployment is expected to be more severe, which should be avoided in engineering application.

Effect of asynchronous release of torsion springs on the deployment of PhoneSat

To guarantee the synchronous deployment of deployable mechanism of large spacecraft, synchro-mechanism such as close cable loop has been widely adopted. However, taking the strict mass, volume and size restrictions imposed by the small satellite into consideration, synchro-mechanism used for large satellites may not be suitable for small satellites any more. As a matter of fact, there is no such mechanism on small-scale satellites to ensure a sufficient level of deployment synchronicity to satisfy the requirement of light weight and simple design. Hence, small satellites with deployable appendages are highly vulnerable to asynchronous deployment owing to the time interval of the detonation of explosive bolts, which deserves a detailed analysis. To evaluate the effect of deployment asynchronicity on the attitude of the PhoneSat during the deployment, simulations are carried out assuming different deployment time lag from 1 to 3 s.

Figure 5 shows the deployment response of the PhoneSat with different deployment time lag. As expected, the deployment time lag has extraordinarily obvious influence on the time necessary to complete the deployment maneuver and damp out residual oscillations, as can be seen in the Figure 5 (a), (c) and (e). Moreover, it can also be found that the deployment time lag has a slight effect on the attitude angular velocity of the PhoneSat after deployment. As shown in

Figure 5 Attitude angles of the PhoneSat

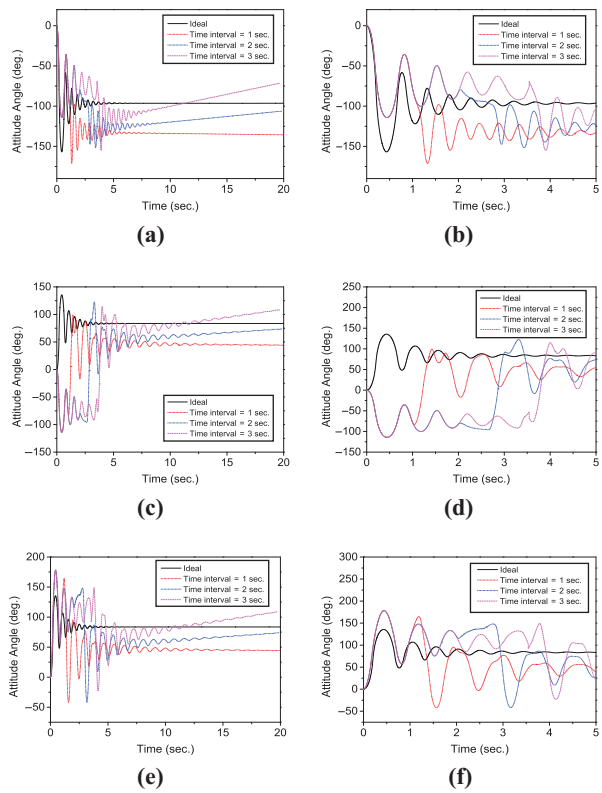

Notes: (a), (c) and (e) are the whole process drawing of Body-1, Body-2 and Body-3, respectively; (b), (d) and (f) are the partial enlarged drawing of the beginning of the deployment of Body-1, Body-2 and Body-3, respectively

Figure 5 (a), (c) and (e), the PhoneSat is left with an increasing magnitude of angular velocity at the end of the deployment with increasing lag time. With the time lag of 1 s, the angular velocity at the end of the deployment is about 0.18°/s, whereas with the time lag of 3 s, the angular velocity left at the end of the deployment is about 2.9°/s.

The attitude motions of three panels in the first 5 s are shown in Figure 5 (b), (d) and (f) to better classify the dynamic characteristics of the unsynchronized deployment. At the beginning, the explosive bolt in Joint-3 detonates, resulting in the deployment of Body-3 driven by the torsion spring in Join-3, whereas Body-2 is still in the folded state because of the time lag of the detonation. Thus, the overall deployment is much like "two" panels oscillating together before the detonation of the other explosive bolt, for the attitude motion of Body-1 is continuously consistent with that of Body-2, whereas the amplitudes of oscillation of all panels gradually decrease because of the damping of spring and friction, as can be seen in the figure. Until the detonation of the other explosive bolt, the relatively stable state has been completely altered. As shown in the figure, the abrupt change of the attitude of three panels indicates that Body-1 is beginning to deploy. After that, the attitude motion of Body-2 is separating from that of Body-1, and, at the same time, the deployment of Body-2 also cause large disturbances to Body-3 which originally tends to stabilize. It can be seen from Figure 5 (a), (c) and (e), long-term residual oscillations remain after the release of Join-2, slowly damped out by hinge friction and spring. Therefore, deployment time lag arising from deployment maneuvers is not expected to be large enough to generate large oscillations of the spacecraft to assure a sufficient level of reliability of the passive deployment.

Effect of initial disturbance angular velocity on deployment of PhoneSat

In most cases, the deployment of small satellites is studied in the common mode, i.e. the satellite is released without initial angular velocity. However, the presence of initial disturbance angular velocity is inevitable because of the imperfect release process, which has a significant effect on the deployment of small satellites. In this section, to analyze the influence of initial disturbance angular velocity, the simulations of PhoneSat with different initial angular velocities are presented.

First, the simulation is conducted with four cases, in which the initial angular velocity of PhoneSat are all along the direction of deployment, i.e. along the X_0-axis of the inertial frame, ranging from 0 to 30°/s at steps of 10°/s. For the sake of clarity in the graphs, only the attitude angle and angular velocity of Body-1 and Body-2 are plotted, owing to the fact that the deployment response of Body-3 is substantially the same as that of Body-2. As can be seen in the Figure 6 (a) and (c), the initial disturbance angular velocity does not significantly affect the time for deployment. It can be seen that the most relevant difference with respect to the deployment without initial angular velocity is that all the simulations with initial angular velocity resulted in the PhoneSat having a constant angular velocity about the X_0 axis at the end of the deployment process. The angular velocity of PhoneSat is shown in Figure 6 (b) and (d) to better clarify the dynamic

Figure 6 Attitude motion of the PhoneSat

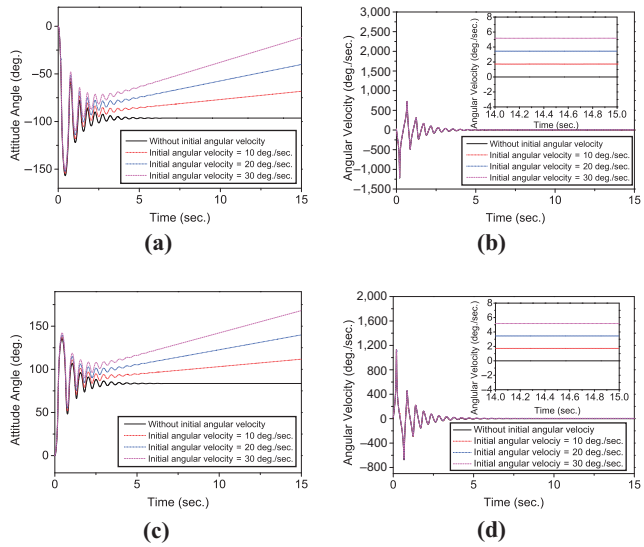

Notes: (a) and (c) are the attitude angles of Body-1 and Body-2, respectively; (b) and (d) are the angular velocities of Body-1 and Body-2, respectively

response of PhoneSat during the deployment. The constant angular velocity after the deployment could be better evidenced in the partial enlarged drawing in Figure 6 (b) and (d), where the magnitudes of the post-deployment angular velocity are 1.7, 3.4 and 5.1°/s when the initial disturbance angular velocity are 10, 20 and 30°/s, respectively. It is observed that the ratio between the magnitude of post-deployment angular velocity and that of pre-deployment angular velocity is a constant with a value of 0.17, which is exactly the ratio between the moment of inertia in the folded state and that in the deployed state, owing to the conservation of angular momentum. It indicates that the effect of the initial disturbance angular velocity in the direction of deployment is weakened to a certain extent because of the deployment of the PhoneSat, causing the inertia tensor in the direction of X_0 axis to increase. Thus, it can be concluded that the initial disturbance angular velocity in the direction of deployment has no disturbance on the attitude of PhoneSat except inducing the post-deployment angular velocity, which is proportional to the initial disturbance angular velocity.

To analyze a more general case, the case that initial angular velocity is along the direction of Y_0-axis of the inertial frame is assumed, with the value of initial angular velocity being 10°/s. The angular velocities of Body-1 and Body-2 are shown as Figure 7. In this case, the effects of the initial disturbance angular velocity are evident. As can be seen from Figure 7, although the direction of initial angular velocity is along Y_0-axis, angular velocities along other two axes are induced during the deployment. At the end of the deployment, the PhoneSat is left with the angular velocity of 0.32, 4.6 and 0.32°/s about X_0, Y_0 and Z_0 axis, respectively, which causes the attitude angle to increase steadily. It can be concluded that the initial disturbance angular not in the direction of deployment induces the angular velocities of the other axes,

Figure 7 Attitude motion of the PhoneSat

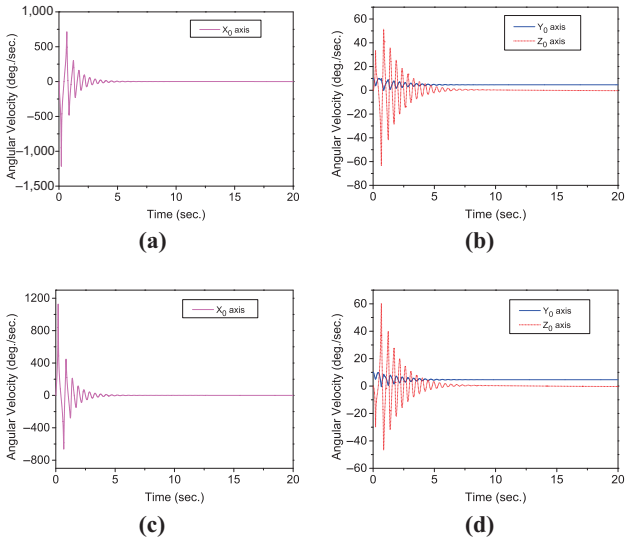

Notes: (a) and (b) are the attitude velocities of Body-1 in three axes, respectively; (c) and (d) are the attitude velocities of Body-2 in three axes, respectively

which dramatically enhances the complexity of attitude control.

Conclusion

This work investigates the influence of joint friction, asymmetry of the spring stiffness, deployment asynchronicity and initial disturbance angular velocity on the attitude of a Z-folded PhoneSat during and after deployment. The dynamic model of the NPU-PhoneSat, a foldable picosatellite consisting of three modules unfolded by passively deployed torsion springs, is established, taking the friction model into consideration. And then, the numerical simulation of the deployment of the PhoneSat is presented and discussed to analyze the effects of the disturbance factors mentioned above.

The results indicate that all the disturbance factors mentioned above have obvious influence on the dynamics response of the PhoneSat in deployment. Friction has a main contribution to reducing the oscillation of attitude motion and damping out the residual oscillation, ultimately decreasing the deployment time, whereas the post-deployment attitude is barely affected. An increasing length of time for the complete deployment is required with the increasing stiffness asymmetry and time difference of asynchronous deployment. In addition to inducing high amplitudes of oscillation, stiffness asymmetry and deployment asynchronicity have slight disturbances on the attitude angle and angular velocity of PhoneSat at the end of the deployment, respectively. The initial disturbance angular velocity has no major effects on deployment time, but its direction has an extraordinary impact on the post-deployment angular velocity. The initial disturbance angular velocity in the direction of deployment would be proportionally weakened at the end of the deployment owing to the increase of inertia tensor in the same direction, whereas initial disturbance angular velocity not in the direction of deployment induces angular velocities of other axes, which dramatically enhances the complexity of attitude control. The results providing valuable data for the influence of those factors on the attitude motion during and after deployment. Our study opens avenues for the next generation of attitude correction strategy especially suitable for nanosatellites with strict volume, mass and power constrains.

References

Calassa, M.C. and Kackley, R. (1995), "Solar array deployment mechanism", paper presented at the 29th Aerospace Mechanisms Symposium.

Campbell, D., Barrett, R., Lake, M.S., Adams, L., Abramson, E., Scherbarth, M.R. and Abbot, J. (2006), "Development of a novel, passively deployed roll-out solar array", paper presented at the IEEE Aerospace Conference, 2006.

Clark, C. and Kirk, S. (2012), "Off-the-shelf, deployable solar panels for CubeSats", paper presented at the CubeSat Developers' Workshop 2012.

Cockrell, J., Alena, R., Mayer, D., Sanchez, H., Luzod, T., Yost, B. and Klumpar, D. (2012), "EDSN: a large swarm of advanced yet very affordable, COTS-based NanoSats that enable multipoint physics and open source apps".

Fufa, B., Zhao-Bo, C. and Wensheng, M. (2010), "Modeling and simulation of satellite solar panel deployment and locking", *Information Technology Journal*, Vol. 9 No. 3, pp. 600-604.

Gao, E.W., Zhang, X.P. and Yao, Z.Q. (2008), "Simulation and analysis of flexible solar panels' deployment and locking processes", *Journal of Shanghai Jiaotong University (Science)*, Vol. 13, pp. 275-279.

Gerlach, L., Fournier-Sicre, A., Fromberg, A. and Kroehnert, S. (1990), "Hubble space telescope solar generator design for a decade in orbit", paper presented at the Photovoltaic Specialists Conference, 1990.

Heidt, H., Puig-Suari, J., Moore, A., Nakasuka, S. and Twiggs, R. (2000), "CubeSat: a new generation of picosatellite for education and industry low-cost space experimentation".

Hong, J.Z. (1999), *Computational Dynamics of Multibody Systems*, Higher Education Press, Beijing.

Jaeger, T., Ciffone, M. and Anden, E. (2011), "Mayflower: Next generation CubeSat flight testbed".

Jansen, T., Reinders, A., Oomen, G. and Bouwmeester, J. (2010), "Performance of the first flight experiment with dedicated space CIGS cells onboard the Delfi-C3 nanosatellite", paper presented at the IEEE Photovoltaic Specialists Conference (PVSC), 2010.

Kote, A., Balaji, K., Nataraju, B. and Aralimatti, V. (2007), "Effect of solar array deployment on spacecraft attitude", *Journal of Spacecraft Technology*, Vol. 17 No. 2, pp. 1-8.

Lee, K. (2005), "Solar array deployment qualification for the LMX line of buses", paper presented at the 11th ESMATS Symposium, European Space Agency (ESA).

Piattoni, J., Candini, G.P., Pezzi, G., Santoni, F. and Piergentili, F. (2012), "Plastic Cubesat: an innovative and low-cost way to perform applied space research and hands-on education", *Acta Astronautica*, Vol. 81 No. 2, pp. 419-429.

Plaza, J.M.E., Vilán, J.A.V., Agelet, F.A. and Barandiarán, J. (2010), "Xatcobeo: small mechanisms for CubeSat Satellites–Antenna and Solar Array Deployment", paper presented at the 40th Aerospace Mechanisms Symposium, NASA Kennedy Space Centre.

Reif, A.W., Hoang, V. and Kalman, A.E. (2010), "Recent advances in the construction of solar arrays for CubeSats", paper presented at the CubeSat summer developer's workshop, Proceedings of the 24th Annual AIAA/USU Conference on Small Satellites, UT State University.

Santoni, F. (2014), "Dynamics of spring-deployed solar panels for Agile Nanospacecraft", *Journal of Aerospace Engineering*, p. 04014122.

Santoni, F. and Piergentili, F. (2008), "Analysis of the UNISAT-3 solar array in-orbit performance", *Journal of Spacecraft and Rockets*, Vol. 45 No. 1, pp. 142-148.

Santoni, F., Piergentili, F., Donati, S., Perelli, M., Negri, A. and Marino, M. (2014), "An innovative deployable solar panel system for Cubesats", *Acta Astronautica*, Vol. 95, pp. 210-217.

Wallrapp, O. and Wiedemann, S. (2002), "Simulation of deployment of a flexible solar array", *Multibody System Dynamics*, Vol. 7 No. 1, pp. 101-125.

Wie, B., Furumoto, N., Banerjee, A. and Barba, P. (1986), "Modeling and simulation of spacecraft solar array deployment", *Journal of Guidance, Control, and Dynamics*, Vol. 9 No. 5, pp. 593-598.

Yuan, J.P., Qiao, Q., Yuan, J., Shi, Y., Hou, J., Li, S., Shi, S., Li, L., Gao, R.Z.W., Liu, Y. and Sun, H. (2015), "The design of NPU-PhoneSat: a Foldable Pico Satellite using Smart Phone Thechnology", paper presented at the 25th AAS/AIAA Space Flight Mechanics Meeting.

Aircraft Engineering and Aerospace Technology: An International Journal
Volume 89 · Number 3 · 2017 · 498–506

Corresponding author

Qiao Qiao can be contacted at: doubleqiao1992@outlook.com